Nitrogen-pair paramagnetic defects in diamond: A density functional study

K. M. Etmimi, M. E. Ahmed, P. R. Briddon, J. P. Goss,* and A. M. Gsiea
School of Electrical, Electronic, and Computer Engineering, Newcastle University, Newcastle upon Tyne NE1 7RU, England, United Kingdom

(Received 21 November 2008; revised manuscript received 24 March 2009; published 14 May 2009)

The N1, W7, M2, N4, M3, and NOC1-4 electron-paramagnetic-resonance centers in diamond have been assigned to pairs of nitrogen donors separated by different numbers of intervening host sites, both in ionized, $S=1/2$, and neutral $S=1$ forms. Using density functional techniques, we confirm these models, but in order to do so for the N4 center we show that it is essential that extremely low energy reorientation takes place. We also show that charge exchange and chemical rebonding effects provide an explanation for the distinct forms of $S=1$, neutral configurations observed.

DOI: 10.1103/PhysRevB.79.205207 PACS number(s): 61.72.J−, 61.72.Bb, 71.20.Mq, 71.23.An

I. INTRODUCTION

Natural diamonds are classified by nitrogen content,[1] with type-Ia labeling those which contain nitrogen in an aggregated form, and type-Ib containing N as isolated impurities (N_s^0), sometimes labeled as C-centers [Fig. 1(b)]. Nitrogen aggregates are principally of A and B form, and the A-center structure is also illustrated in Fig. 1(d). The driving force for aggregation is the reduction in energy concomitant with the removal of carbon radicals associated with N_s^0. We previously showed the formation energies per N atom of A and B centers are 2.0 and 2.9 eV lower than the C-center.[2]

N_s^0 is well characterized. It possesses an unpaired electron and is observed as the P1 electron-paramagnetic resonance (EPR) center.[3] Analysis of the hyperfine interaction[3] with the ^{13}C and ^{14}N species in P1 suggests 67% and 25% of the spin-density is associated with the central C and N atoms, respectively, consistent with the band-gap orbitals being a carbon radical and nitrogen lone pair. The neutral and ionized forms also give rise to vibrational modes[4,5] at 1344 cm^{-1} and 1332 cm^{-1}, respectively.

A-centers are also characterized by vibrational modes resonant with the diamond host phonons and seen as broad peaks in infrared.[6] Indeed, the labels A, B, and C for different forms of nitrogen in diamond originates from labeling of IR absorption bands. In contrast with C-centers, A-centers have only paired electrons and are EPR inactive. However, they may be photoionized (with an activation energy[7] of 3.8 eV), and in the positive charge state give rise to the W24 EPR spectrum.[8,9]

In addition to ionized A-centers, five $S=1/2$ EPR centers have been attributed to pairs of N atoms, but separated by a number of intervening host sites. The N1,[10,11] W7,[12–14] M2,[15,16] N4,[17,18] and M3 (Refs. 15 and 16) EPR centers have models comprised from substitutional nitrogen atoms at second to sixth shells of neighbor sites, respectively, as labeled in Fig. 2. In contrast to W24, the ionized state does not require illumination.

Configurations of nearby P1-centers adopting a $S=1$ spin state have also been detected: NOC-1, NOC-2, NOC-3, and NOC-4 EPR centers.[19] Models for these centers are C-centers at fourth, seventh (or ninth), and tenth shells for NOC-1, NOC-2, and NOC-3, while NOC-4 is a superposition of spectra from more distant pairs.

Previously, we analyzed N pairs as part of a broader study into the stability of impurity pairs in diamond.[20] In the present study we focus on the expected hyperfine interactions for the proposed dissociated, ionized nitrogen-pair models, and by analyzing the reorientation barriers, revise the models. We also investigate the origin of the cases of $S=1$ combinations of close by P1-centers. In so doing, we explain why only some combinations are seen.

II. METHOD

Calculations were carried out using the spin-density-functional technique, implemented in AIMPRO (Refs. 21 and 22) (*ab initio* modeling program), with the Perdew, Burke,

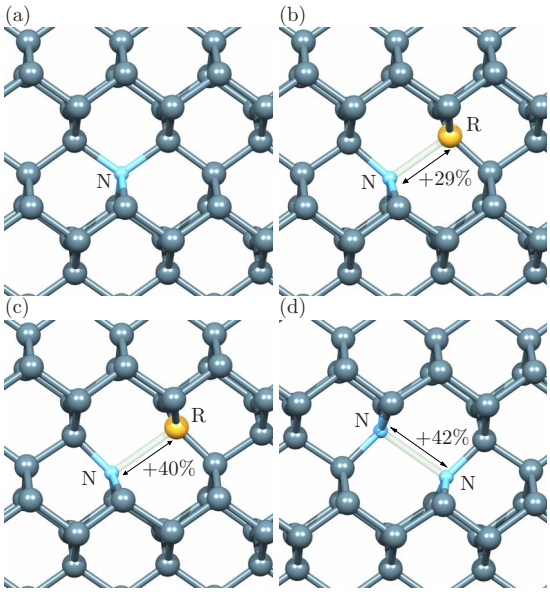

FIG. 1. (Color online) Schematics showing the calculated structures of nitrogen defects in diamond. (a) The ionized C-center (N_s^+), (b) the neutral C-center (N_s^0), (c) the negatively charged C-center (N_s^-), and (d) the A-center. Labeled sites are N for nitrogen and R indicating the carbon radical or anion site. Horizontal and vertical directions are approximately [110] and [001], respectively. Percentages indicate the calculated extension of the respective interactions over that of the host C-C bond length.

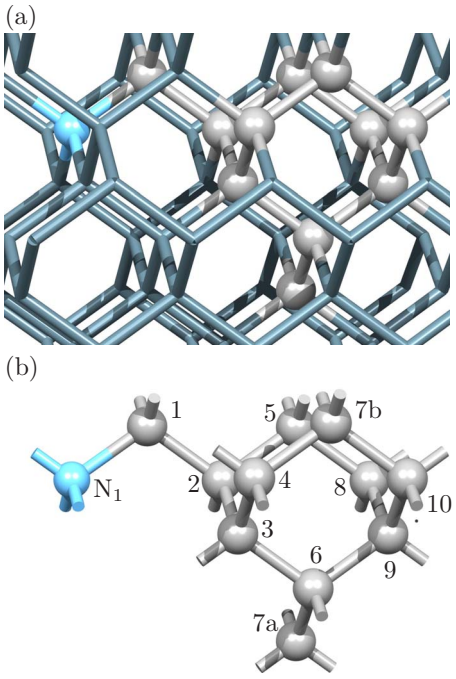

FIG. 2. (Color online) Schematics showing shells of neighbors in diamond. (a) shows the sites embedded in the diamond lattice, with (b) showing just prototypical sites for each shell of neighbors relative to the first nitrogen site, N_1. The two types of seventh-shell site are labeled 7a and 7b in accord with Ref. 19.

and Ernzerhof generalized-gradient approximation.[23]

The wave function basis consists of atom-centered Gaussians.[24] Carbon is treated using fixed linear-combinations of *s* and *p* orbitals with the addition of a set of *d* functions to allow for polarization, with a total of 13 functions per atom. Nitrogen is treated using independent sets of *s*, *p*, and *d* Gaussians with four widths, yielding 40 functions per atom. The charge density is Fourier-transformed using plane waves with a cutoff of 350 Ry, yielding well converged total energies. Core electrons are eliminated by using norm-conserving pseudopotentials.[25] The lattice constant and bulk modulus of bulk diamond are, respectively, reproduced to within ~1% (an overestimate) and 2% (underestimate) of experiment. The calculated direct and indirect band gaps agree with published plane-wave values.[26]

Generally 216-atom, simple-cubic supercells of side length $3a_0$ are used. This ensures the N atoms are closer to one another than any of the periodic images. For tenth-shell pairs, this is insufficient, and here we use a 256-atom cell with body-centered-cubic lattice vectors. In all cases we sample the Brillouin zone using the Monkhorst-Pack scheme,[27] using a sampling density of 0.64×10^{-3} Å^{-3} per point or better. We estimate an error in the relative energies of different structures due to Brillouin-zone sampling of <10 meV.

Hyperfine interactions are modeled as outlined previously.[28] Briefly, this involves the combination of pseudopotentials and reconstructed all electron wave functions in the core region.[29,30] Reconstruction of the ion cores allows us to calculate the hyperfine tensor elements within a frozen-core all-electron wave function approximation, without the computational difficulties associated with a full all-electron calculation. In the text we also present simplified terms A_s and A_p for the isotropic and anisotropic components of a hyperfine tensor. In the case of axially symmetric tensors, these are given by $(A_\parallel + 2A_\perp)/3$ and $(A_\parallel - A_\perp)/3$, respectively, where $A_\parallel$ is the magnitude of the component along the axial direction and $A_\perp$ that of the two components perpendicular to the axis. Where the symmetry is only approximately axial, A_p is calculated using $A_\perp$ taken as the average of the two nearly degenerate terms. In this paper we quote hyperfine tensors calculated for ^{13}C and ^{14}N. In the latter case, the ^{15}N values can be obtained from those of ^{14}N simply by multiplication by -1.32, a factor given by the ratio of nuclear magnetic moments divided by the corresponding nuclear spins.[31] The calculated directions are unaffected by isotope. For the calculated hyperfine interactions, an enhanced carbon wave function basis consisting of 28 functions per atom is used to ensure a reasonable level of convergence. Increasing the basis further to 40 functions per atom leads to small changes in the calculated structures and hyperfine tensors: for example for $(N3N)^+$, the tensor elements for all of the carbon-sites analyzed are within around 1 MHz of those of the smaller basis.

Electrical levels are obtained by use of the marker method.[24] In this report the donor levels are obtained in comparison to N_s^0 with a level at $E_c - 1.7$ eV.[32]

Reaction energies are obtained using the climbing nudged-elastic-band (NEB) method.[33,34] We use a minimum of five images, and optimize the barrier so that image-forces are less than 0.01 a.u. and the saddle-point energy changes by less than 1 meV. Due to the computational cost, the barriers are obtained using cubic unit cells of side length $2a_0$, unless specified otherwise. In specific cases we examined the effect of cell size on barrier height and we are satisfied that the smaller cell yields values within 10 s of meV of the larger.

III. COMPUTATION RESULTS

Substitutional nitrogen pairs at increasing distances are modeled. In each case we investigate geometry, electronic structure, electrical activity, reorientation barriers and, for $S = 1/2$ systems, the hyperfine interactions. For neutral pairs, we have optimized starting from all combinations of pairs of dilated N-C "bonds," one broken-bond per N site. We have examined $S=0$ and $S=1$ configurations, with the potential antiferromagnetic interaction where the two N sites are of opposite spin. We have also initiated relaxation starting from $N_s^+ \ldots N_s^-$ where there is a single broken bond. Finally, throughout this paper we have adopted the notation that N pairs in the n^{th} shell (Fig. 2) are labeled N*n*N. The results are presented in order of increasing N-N separation.

A. First-shell pairs and W24

N1N has been examined previously, and we review only the main points here. The relaxed structure results in a significant dilation of the N-N distance relative to that of the host C-C bond length, as indicated in Fig. 1(d). All atoms are

TABLE I. Hyperfine tensors (MHz) for ^{14}N and their six ^{13}C neighbors in $(N1N)^+$. Directions are indicated in parentheses using spherical polar coordinates (Ref. 35). Experimental data for W24 are taken from Ref. 36. All calculated data are rounded to the nearest MHz or degree.

Site	A_1		A_2		A_3		A_s	A_p
				Calculations				
^{14}N	156	(125,45)	74	(57,343)	74	(53,103)	101	27
^{13}C	−13	(90,315)	−12	(9,225)	−8	(81,45)	−11	
				Experiment (W24)				
^{14}N	155.26	∥ [111]	81.51	⊥ [111]	81.51	⊥ [111]	106.09	24.58
^{13}C							12.3	

coordinated according to their valence, and the band gap is devoid of the partially filled states characteristic of the nitrogen donor. Above the valence band top lies an occupied-state associated with the nitrogen lone-pair orbitals. We note in passing that there are metastable forms of N1N containing a N-N bond and two carbon radicals. However these are >4 eV higher in energy than the A-center and are of no practical importance.

Photoionization of N1N yields the W24 EPR center.[8,9] We find ionization reduces the dilation of the N-N separation from 42% to 31%, but the N atoms remain equivalent[37] and the overall symmetry is D_{3d}. The calculated hyperfine interactions for the N atoms and their six equivalent carbon neighbors are presented in Table I. The agreement with experiment is excellent, lending confidence both to the assignment of W24 to the ionized A-center, and to the values presented for the dissociated N pairs presented below. The sign of A_s for ^{13}C is not known experimentally, but we predict it to be negative.

The ease with which N1N is ionized may be estimated from two sets of data. As a purely qualitative picture, the Kohn-Sham band structure (not plotted) shows an absence of any bands deep in the gap, which would be consistent with the need for illumination to ionize the A-center. A more quantitative approach is to calculate the ionization level relative to a marker system:[24] the donor level of an A-center is calculated to lie 2.0 eV lower than that of a C-center, locating it at $E_c-3.7$ eV. This deep level is in excellent agreement with the experimental[7] value of $E_c-3.8$ eV.

B. Second-shell pairs and N1

There are several metastable structures for N2N, but the lowest in energy exhibits a *single* dilated N-C bond, shown schematically in Fig. 3. The on-site location for one N atom may indicate that N2N adopts a N_s^--C-N_s^+ form. The next most stable structure is 0.5 eV higher in energy, with $S=1$ and two dilated bonds.

The N1 EPR center has been assigned[38] to $(N2N)^+$. In support, we find N2N easier to ionize than an A-center, with a donor level at $E_c-1.9$ eV. Then midgap acceptors, such as vacancies,[39] may ionize these defects without the need for illumination. An effect of ionizing N2N is a reduction in the broken N-C dilation from 41% in the neutral charge state to 30% in the positive charge state. This is close to the calculated reduction in dilation of N_s^- to N_s^0, supporting the view of the charge transfer between the N sites in the neutral charge state of N2N.

The calculated hyperfine tensors for key atoms in $(N2N)^+$ are listed in Table II. Experiment indicates hyperfine tensors for two nonequivalent nitrogen sites in N1, and the agreement between the calculations and measurements is rather good. Additionally, spectra for nearby ^{13}C sites have been reported.[10,38] Perhaps surprisingly, the large hyperfine interaction with the central carbon atom (C_1, Fig. 3) is not one of them, but three more remote types of neighbor are, labeled I, II, and III. Table III lists the calculated values for the isotropic and anisotropic contributions of the hyperfine tensors for carbon sites as labeled in Fig. 3. A good fit to experiment[38] can be made by assigning sites I, II, and III to (C_2+C_2'), C_3, and C_4, respectively.

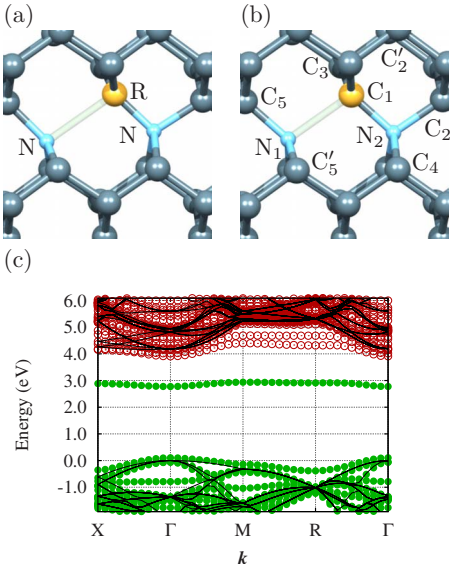

FIG. 3. (Color online) Schematics of N2N in diamond in the (a) neutral and (b) positive charge states. Atom sizes and shading, as well as crystallographic orientation is as in Fig. 1. (c) The Kohn-Sham band structure in the vicinity of the band gap for (N2N). Filled and empty circles show filled and empty bands, respectively, with the bands from the defect-free cell superimposed in full lines for comparison. The energy scale is defined by the valence band top at zero energy ($E_v=0$ eV).

TABLE II. Calculated hyperfine tensors (MHz) for ^{14}N and ^{13}C, for the sites identified in Fig. 3. Tensors are listed as in Table I, and the experimental data for N1 are taken from Ref. 11.

Site	A_1		A_2		A_3	
			Calculations			
$^{14}N_1$	124	(55,45)	80	(35,224)	80	(90,135)
$^{14}N_2$	−7	(90,135)	−7	(23,45)	−7	(67,225)
$^{13}C_1$	408	(54,45)	200	(90,315)	199	(36,225)
			Experiment (N1)			
$^{14}N_1$	126.36	(55,45)	89.20	(35,225)	89.22	(90,135)
$^{14}N_2$	−8.33	(90,135)	−8.29	(20,45)	−7.88	(70,225)

It is perhaps surprising that C_2 and C_2' have numerically indistinguishable hyperfine tensors, given that C_2 has a N neighbor, and the others do not. We note that for the C_4 sites in Fig. 3, if we disregard N_2, there are an additional four sites symmetrically arranged relative to the N_1-C_1 axis. However, the computed values of A_s and A_p for the four additional sites are around half that of C_4, and as such should be distinguishable in experiment.

Our assignment of ^{13}C sites partially agrees with the interpretation of experiment. Due to the overall planar symmetry of the defect, the number of equivalent sites can be only 1 or 2, and not 3. For assignment of three equivalent ^{13}C in site I, we would have to combine the unique C_2 and the two labeled C_2' in Fig. 3(b). However, the calculated values for these inequivalent sites are numerically the same, and thus we agree with this assignment, despite the C_2 and C_2' sites being inequivalent by symmetry. The assignment of the experimental site III to the two C_3 sites is also in accord with the calculations. However, type II sites have to be reassigned to C_4 from C_5+C_5', for which we find very small hyperfine interactions, which requires a change in the number of equivalent C-sites from 3 to 2.

TABLE III. ^{13}C hyperfine for sites in N2N (Fig. 3), and those obtained experimentally for the N1 EPR center, with labels and values taken from Refs. 10 and 38. *n* indicates the number of equivalent sites in each case.

Site	A_s	A_p	*n*
Calculations			
C_1	269	70	1
C_2	29	3	1
C_2'	29	3	2
C_3	−21	~1	2
C_4	14	2	2
C_5	−6	1	1
C_5'	−6	1	2
Experiment (N1)			
I	28.3	2.6	3
II	21.3	0.6	3
III	16.7	1.1	2

We also examined the reorientation barriers, yielding 1.4 and 0.7 eV in the neutral and positive charge states, respectively. Experimentally, the reorientation barrier for N1, assigned to the positive charge state, has been measured[11,40] to be 0.4 eV.

The apparently large difference between the calculation and experiment is mitigated by two factors. First, the calculation is classical in nature, and quantum-mechanical effects such as tunneling would tend to lower the effective barrier. Indeed, the distance traveled by the radical site is small and it remains on the same C atom throughout the process; by calculating the total displacement vector of all species through the reaction, we determine the barrier to be less than 0.6 Å in width. The calculation of a tunneling factor would be of some interest, but is beyond the scope of this study. Second, there is only a single measurement of the activation energy, and the uncertainty in the value is not clear.

Noting both these arguments and the excellent agreement of the calculated hyperfine tensors with the experimental data, the barrier height may be viewed as in tolerable agreement with experiment. It is certainly not so much in error as to preclude the assignment of the model to the EPR center. We shall show later that the calculated activation energies for other N-pair configurations are somewhat different from that for $(N2N)^+$, and overall the trend in the energetics fits well with observation.

In summary, combining the ground-state structures, hyperfine interaction data, ionization energy, and to a lesser extent the reorientation barrier, we conclude that the quantum-chemical modeling agrees with the assignment of N1 to $(N2N)^+$, subject to revision of the assignments for nearby carbon hyperfine interactions and number of equivalent sites.

C. Third-shell pairs and W7

The most stable structure found for N3N has C_2 symmetry and is shown in Fig. 4(a). In contrast with N2N, each N site has an associated broken N-C bond, and this is favored in this case as the neighboring carbon radicals form a partial p_π bond. The rebonding renders it 0.5–0.8 eV more favorable than other metastable structures.

The corresponding band structure is plotted in Fig. 4(c). Again, it contrasts with that of N2N [Fig. 3(c)], with both occupied and unoccupied bands lying well within the band-gap. These roughly correspond to p_π and p_π^* combinations of the two C-radical sites.

Upon ionization, one broken-bond reforms, leaving a paramagnetic center resembling a perturbed P1 defect. This $S=1/2$ complex has been assigned to the W7 EPR center,[38] and in Table IV we report the calculated hyperfine interactions in comparison to the measured values.

The agreement in both magnitude and direction for the N_s^0 component is good. Furthermore, the directions for the ionized N site are reasonable, and the isotropic components computed at 18 MHz agree well with the measured value of 15 MHz. We conclude that the calculations are consistent

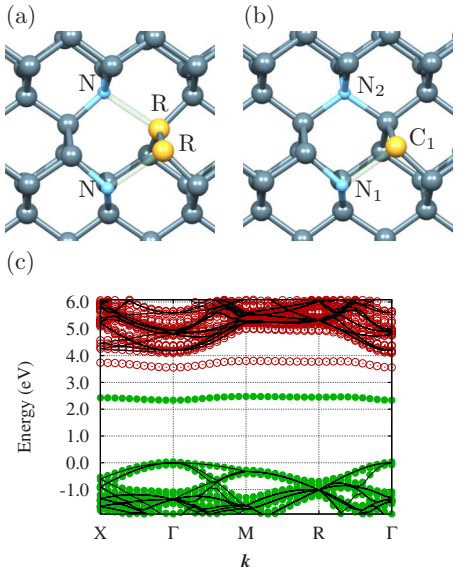

FIG. 4. (Color online) Schematics of the N3N complex in diamond in the (a) neutral and (b) positive charge states. (c) The Kohn-Sham band structure in the vicinity of the band gap for (N3N). Symbols, axes, and scales are as indicated in Fig. 3.

with the $(N3N)^+$ model for the W7 EPR center.

Loubser and Wright[13] noted that for measurements between 77 K and room temperature, motional effects became important. They interpreted their data as a reorientation barrier of 0.24 eV ± 0.01 eV. The process of reorientation in the case of $(N3N)^+$ is somewhat more complicated than for N2N as there at least three different reorientation reactions resulting in a symmetrically equivalent product, as illustrated in Fig. 5.

We have calculated barriers in three cases. The lowest energy is path (i), at 0.18 eV, with path (ii) activated by 0.40 eV. Trajectory (iii) is not favored, with a route made up from path (i)+(ii) [or equivalently (ii)+(i)] energetically preferred. We therefore predict that reorientation will occur in two stages. The first activation involving path (i) results in an average structure with C_2 symmetry, similar to the structure in Fig. 4(a). At higher temperatures path (ii) becomes accessible and the effective symmetry is raised to C_{2h}. Since the radical site is moving in this case (contrasting with N2N), the impact of quantum tunneling is likely to be reduced. The barriers are in good agreement with the experimental estimate, lending further support to the model.

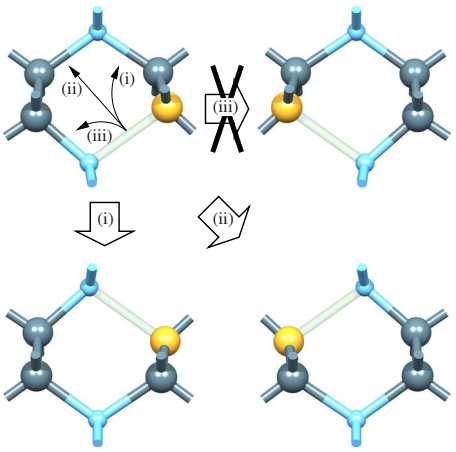

FIG. 5. (Color online) Schematic showing three modes for reorientation as discussed in the text for $(N3N)^+$. Colors and orientation are as in Fig. 1.

TABLE IV. Calculated hyperfine tensors (MHz) for ^{14}N and ^{13}C, for the sites identified in Fig. 4. Experimental data taken from Ref. 14. Notation is as in Table I. The motional averages are indicated as the dynamic values for A, with the two cases as indicated in the text.

Site	A_1		A_2		A_3	
			Calculations (static)			
$^{14}N_1$	116	(125,134)	77	(89,45)	77	(35,136)
$^{14}N_2$	20	(56,74)	17	(116,3)	17	(45,303)
$^{13}C_1$	378	(55,315)	179	(80,52)	179	(37,155)
Calculations (dynamic, C_2)						
$^{14}N_1$	68	(53,46)	47	(131,94)	47	(116,338)
Calculations (dynamic, C_{2h})						
$^{14}N_1$	60	(90,45)	55	(2,135)	47	(92,135)
			Experiment (W7)			
$^{14}N_1$	121.39	∥ [111]	86.00	⊥ [111]	86.00	⊥ [111]
$^{14}N_2$	16.01	(66,71)	14.00	(123,358)	13.58	(42,313)

Table IV also lists hyperfine tensors where motional averaging is applied. Neither yield values resembling the experimental values for W7, supporting the assignment to a static geometry.

Finally, we note that as with the N2N complex, the band structure [Fig. 4(c)] is suggestive of a donor level in the upper part of the band gap, and the calculated donor level for N3N is estimated to lie around $E_c-2.1$ eV. The increase in ionization energy can be traced to the stabilization of the neutral system due to the partial p_π-bonding interaction between dangling bond orbitals.

In conclusion, combining structure, electrical, motional, and hyperfine data, the calculations support the assignment of W7 to a static $(N3N)^+$ structure.

D. Fourth-shell pairs: NOC-2 and M2

Fourth-shell neighbors lie along the cube directions. Two substitutional nitrogen atoms paired in such a configuration are shown schematically in Fig. 6. As with N3N, we find a structure maintaining two C radicals is most stable, however in this case there is not a single minimum energy structure.

C_{1h} and C_2 symmetry, $S=0$ structures shown in Figs. 6(a) and 6(b) are within a 50 meV of each other, with the planar structure being the most stable. Structure (c) in an $S=1$ state is the model for NOC-2, and this is calculated at 60 meV higher in energy than the diamagnetic form. We shall return to this center in Sec. IV C. These energy differences are small, and it is not clear which of these structures is the true

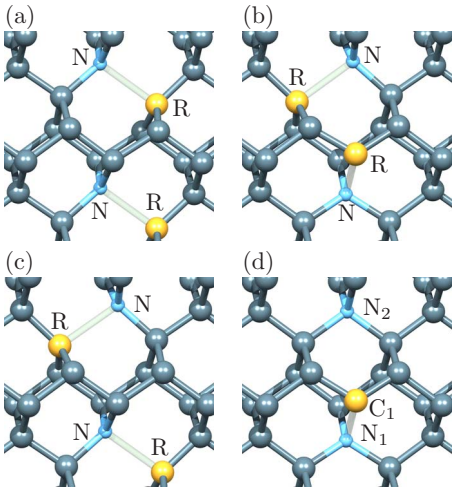

FIG. 6. (Color online) Schematics of the N4N complex in diamond. (a) and (b) show two forms of the neutral, $S=0$ state, (c) the $S=1$ configuration assigned to NOC-2, and (d) the lowest energy structure in the positive charge state. Structures are presented as indicated in Fig. 1.

ground state. We note that the case where the radical sites are most distant is higher in energy by 0.6 eV, in line with a general trend for increasing energy with separation of the radical sites.

In the positive charge state, one N-C bond reforms. The nonequivalence of the N sites yields C_{1h} symmetry, with the lowest energy structure shown in Fig. 6(d). The N centers weakly interact and the calculated donor level is estimated to lie around just 0.1 eV deeper than that of N_s^0. This structure has been assigned to the M2 EPR center,[16] and the calculated hyperfine tensors for $(N4N)^+$ are compared to those of M2 in Table V. The agreement between the P1-like N-site hyperfine and experiment is reasonable, and although the values for the second N site are somewhat overestimated, the directions are in good agreement.

The reorientation of $(N4N)^+$, transferring the unpaired electron between N sites, is found to be activated by 0.3 eV.

TABLE V. Calculated hyperfine tensors (MHz) for ^{14}N and ^{13}C, for the sites identified in Fig. 6(d). Experimental data taken from Ref. 16. Notation is as in Table I. The orientation of the center has been chosen to match the experimental data.

Site	A_1		A_2		A_3	
			Calculations (static)			
$^{14}N_1$	112	(54,45)	75	(90,135)	75	(36,225)
$^{14}N_2$	13	(38,225)	12	(128,225)	12	(90,135)
$^{13}C_1$	374	(55,45)	171	(35,225)	171	(90,315)
			Calculations (dynamic)			
^{14}N	56	(90,45)	50	(0,90)	44	(90,135)
			Experiment (M2)			
$^{14}N_1$	117.95	(54.7,45)	84.48		84.48	
$^{14}N_2$	7.1	(44,225)	6.6	(134,225)	6.6	(90,135)

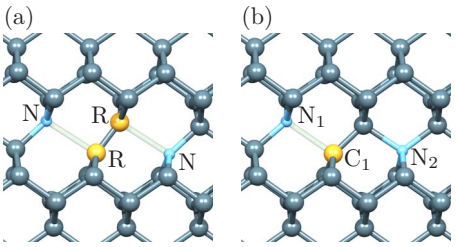

FIG. 7. (Color online) Schematics of the N5N complex in diamond in the (a) neutral and (b) positive charge states. Colors and orientation are as in Fig. 1.

As with the $(N3N)^+$ complex, reorientation about a single N site is not preferred energetically (see Fig. 5), and the calculations suggest that as the temperature increases, there should be a motional averaging from planar (C_{1h}) symmetry to a tetragonal (D_{2d}) center with equivalent N sites. The predicted hyperfine tensors for the motionally averaged system are included in Table V, and they do not resemble the values determined for M2, supporting the assignment of the planar, static structure to the experimental spectrum.

E. Fifth-shell pairs and N4

N5N relaxes to a planar defect (C_{2h} symmetry) with the N sites separated by two reconstructed C-sites, shown in Fig. 7(a). This is particularly stable as the two C-radicals rehybridize, forming a double bond and rendering all atoms fully bonded. The central C-C bond is calculated to be 13% shorter than the diamond C-C bond length, matching the relative C-C bond lengths in ethene and ethane. Configurations where the carbon radicals are arranged differently are considerably higher in energy. For example, where both are perpendicular to the plane containing the N atoms, the total energy is 1.4 eV higher: such geometries are therefore discounted.

Ionization results in a reformed C-N bond, rendering the N-atoms nonequivalent. The calculated donor level is around 0.9 eV below that of N_s^0, it lying deeper in the gap than for the previous cases due to the significantly p_π-bond stabilization in $(N5N)^0$.

The nonequivalence of the N atoms in $(N5N)^+$ has implications in correlating it with the N4 EPR center, which is reported as having equivalent N atoms and no motional averaging.[38] However, the calculated reorientation barrier is very low: just 40 meV. Therefore, even at low temperatures, $(N5N)^+$ will rapidly reorient between equivalent structures, and the observed hyperfine interactions indicating equivalent N sites represent a motional average.

This model is borne out by the calculated hyperfine interactions, as listed in Table VI. Here we present the A-tensors calculated for a static structure, for the saddle-point structure where the N atoms are equivalent by symmetry, and those obtained from averaging the A tensors of $(N_s^0 \ldots C\text{-}C\text{-}N_s^+)$ and $(N_s^+\text{-}C\text{-}C \ldots N_s^0)$. The A tensors for the saddle-point structure are a poor fit to experiment, whereas the motional average is in very good agreement.

From the calculations, it seems clear that motional effects are crucial in the understanding of this center.

TABLE VI. Calculated hyperfine tensors (MHz) for ^{14}N and ^{13}C, for the sites identified in Fig. 7. Experimental data taken from Ref. 38. Notation is as in Table I.

Site	A_1		A_2		A_3	
			Calculations (static)			
$^{14}N_1$	125	(125,45)	80	(90,315)	80	(35,45)
$^{14}N_2$	59	(51,225)	48	(90,315)	48	(39,35)
$^{13}C_1$	336	(125,45)	159	(35,45)	159	(90,135)
			Calculations (saddle point)			
$^{14}N_1$	114	(125,45)	78	(90,315)	77	(35,45)
			Calculations (dynamic)			
$^{14}N_1$	92	(54,225)	64	(90,315)	64	(36,45)
$^{13}C_1$	169	(125,45)	77	(35,45)	75	(90,315)
			Experiment (N4)			
^{14}N	91.3	∥ [111]	65.6	⊥ [111]	65.6	⊥ [111]

Finally, we note the C-C double bond in $(N5N)^0$ leads to a high-frequency local vibrational mode. We estimate for it to lie at 1651 cm^{-1} with A_g symmetry within the C_{2h} point group. Thus it is Raman active and infrared inactive, but it seem unlikely that the concentration of this center would be high enough to detect directly via the local mode.

In summary, invoking a dynamic averaging in the ionized form allows for close agreement between the $(N5N)^+$ structure and the N4 EPR center. Indeed, we conclude that without such an experimentally unresolved motional effect, the measured hyperfine interactions cannot be explained. Such motional averaging, also thought to be important in H-containing defects in diamond,[28] should be considered in the construction of atomic models from experimental data.

F. Sixth-shell pairs and M3

N6N cannot have equivalent N atoms as there are no point group operations that can map the N atoms onto one another, i.e., even under thermal averaging, the N atoms will always be nonequivalent. In contrast to the N3N, N4N, and N5N centers, but in common with N2N, $(N6N)^0$ forms of a $(N_s^-)\ldots(N_s^+)$ charge-transfer complex with a single dilated N-C bond, shown in Fig. 8(a). This structure may be stabilized in this form as the charge resides predominantly on the undercoordinated C site which is geometrically close to the ionized N site. The preference is marginal, however, with an antiferromagnetic combination of $N_s^0(\uparrow)\ldots N_s^0(\downarrow)$ being within 0.1 eV of the ground state. We return to this issue in Sec. IV C.

The calculated donor level for N6N is just 0.1 eV below that of N_s^0, with the lowest energy geometry shown in Fig. 8(b). The M3 EPR center has been correlated[16] with this configuration of $(N6N)^+$, and Table VII lists the calculated hyperfine tensors for comparison.

The barrier for reorientation is calculated at 0.4 eV. All other orientations are found to be 0.10–0.15 eV higher in energy, so at moderate temperatures these alternative orientations would not be significantly populated, and one would expect measured hyperfine tensors to reflect the minimum energy structure.

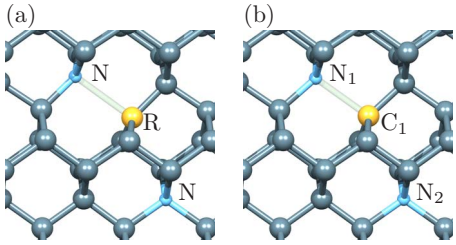

FIG. 8. (Color online) Schematics of the N6N complex in diamond in the (a) neutral and (b) positive charge states. Colors and orientation are as in Fig. 1.

The overall agreement between M3 and the calculations for $(N6N)^+$ is reasonable, but an assignment could not be ambiguously made based solely upon these calculations. However, we note that of the six distinct structures formed by dilating single N-C bonds, that shown in Fig. 8(b), and therefore that with the lowest energy, yields the closest agreement with the M3 EPR parameters. In addition, although the magnitudes calculated for the ionized N component are overestimated, the directions are in good agreement.

To conclude, although the assignment for M3 cannot be definitive, the calculations generally support the model proposed from interpretation of experiment to a sixth-shell N pair.

G. Seventh-shell pairs and NOC-3

In the seventh shell, there are two types of site: one set of four sites along ⟨111⟩ directions, and one set of 12 along ⟨511⟩ directions. We have adopted the 7a and 7b labeling of Nadolinny *et al.*[19] (Fig. 2). We first present the results for type N7aN.

Several combinations of P1 centers for $(N7aN)^0$ are indistinguishable within the energy tolerances of our calculations. The two lowest energy structures are shown in Figs. 9(a) and

TABLE VII. Calculated hyperfine tensors (MHz) for ^{14}N and ^{13}C, for the sites identified in Fig. 8(b). Experimental data taken from Ref. 16. Notation is as in Table I, and the defect crystallographic orientation has been chosen to facilitate comparison with experiment.

Site	A_1		A_2		A_3	
			Calculations			
$^{14}N_1$	116	(55,45)	76	(114,117)	76	(135,0)
$^{14}N_2$	9	(45,180)	10	(132,153)	10	(76,75)
$^{13}C_1$	385	(54,44)	187	(114,116)	187	(135,0)
			Experiment (M3)			
$^{14}N_1$	121.55	(54.7,45)	85.90		85.90	
$^{14}N_2$	5.1	(45,180)	5.4	(133,162)	6.0	(81,81)

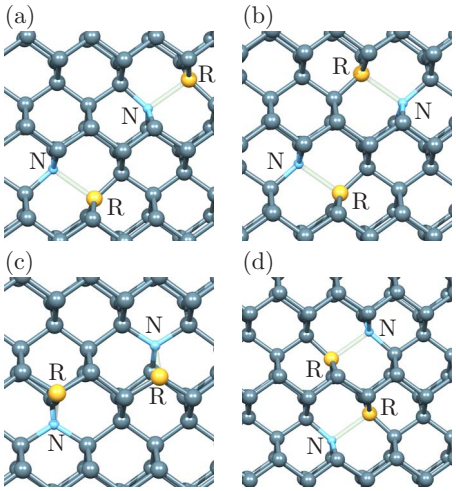

FIG. 9. (Color online) Schematics of the N7aN and N7bN complexes in diamond. (a) and (b) show two energetically degenerate forms of N7aN, with (c) being the model structure for NOC-3. (d) shows the most stable structure for N7bN. Colors and orientation are as in Fig. 1.

9(b), both of which are $S=0$ and approximately degenerate in total energy. The $S=1$ configuration of Fig. 9(b) is degenerate in energy with the $S=0$ ground state, and it may therefore be expected that this orientation should be the one seen in experiment.

According to Ref. 19 the NOC-3 EPR center may arise from one of two structures, and Fig. 9(c) shows their N7aN candidate. However, we find that this geometry and spin state is 0.1 eV above our ground-state configuration, and around 35 meV above the $S=0$ form of this geometry.

We now turn to the second form of seventh neighbor pairs. The most stable N7bN structure, which is shown in Fig. 9(d), is $S=0$ and at least 0.1 eV more stable than any other orientation, in any spin state. The stabilization of this particular form is most likely due to a weak bonding interaction between the parallel radical orbitals.

Since no ionized centers have been assigned to the either seventh-shell structure, and in the interests of brevity, we have not presented any hyperfine data for these centers. However, in brief we note that both forms have ionization energies close to that of isolated N_s^0, and that in the ionized form a single broken N-C bond remains.

H. Eighth-shell pairs

The N-pair defect in the eighth shell, in common with the first and fifth shell pairs, represents a system for which all dangling bonds can be removed in the neutral, $S=0$ state. The structure is shown schematically in Fig. 10(a). The three-member ring is calculated to yield a vibrational mode at around 1480 cm^{-1}, with A_1 symmetry in the C_{2v} point group. This is both infrared and Raman active, but as with N5N it seems likely that the concentrations would be too low for direct detection of this mode.

The formation of the reconstruction yields an electronic structure close to that of the A-center, with no deep bands in the band gap, and filled lone-pair orbitals around the valence band top. This renders the ionization of such a combination rather unlikely: the calculated donor level for N8N is at 1.3 eV deeper than N_s^0, and just 0.6 eV higher than that calculated for the A-center. It would therefore seem likely that, as with the ionization of the A-center to form W24,[9] the ionization of N8N would be favored only under optical excitation.

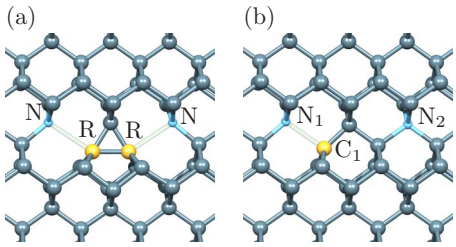

FIG. 10. (Color online) Schematics of the N8N complex in diamond in the (a) neutral and (b) positive charge states. Colors and orientation are as in Fig. 1.

Nevertheless, we present in Table VIII the calculated hyperfine tensors for $(N8N)^+$. The activation energy for migration of the unpaired electron between N sites calculated using a 216-atom supercell is rather low at 0.1 eV. As such, it is possible that if observed, this center would present as a C_{2v} symmetry defect with equivalent N atoms. Table VIII also therefore includes the motionally averaged A tensors for the N atoms and the two C atoms that form the reconstruction in the neutral charge state.

I. Ninth- and tenth-shell pairs: NOC-3 and NOC-1

N9N is a candidate for the NOC-3 EPR center. Indeed, we find the lowest energy structure is in accord with the model proposed for the $S=1$ EPR center, shown in Fig. 11(a). This may suggest that the ninth-shell pairing is more favorable as a model than the seventh shell as a model for NOC-3. However, other configurations and diamagnetic forms are within 20 meV, and we cannot be certain which orientation or spin state is the most stable. An assignment for NOC-3 cannot be confirmed purely on this basis.

The energies separating different orientation and spin-states in N10N are also very small, with 30 meV covering all variants that we examined. In particular, the model structure proposed for NOC-1, shown in Fig. 11(b), is around 10 meV

TABLE VIII. Calculated hyperfine tensors (MHz) for ^{14}N and ^{13}C, for the sites identified in Fig. 10(b). Notation is as in Table I.

Site	A_1		A_2		A_3	
			Static			
$^{14}N_1$	113	(125,45)	76	(35,45)	76	(90,135)
$^{14}N_2$	28	(55,45)	25	(90,315)	24	(35,225)
$^{13}C_1$	376	(53,225)	184	(90,135)	184	(37,45)
			Dynamic			
$^{14}N_1$	69	(57,45)	52	(33,225)	50	(90,315)
$^{13}C_1$	223	(51,225)	128	(39,45)	125	(90,135)

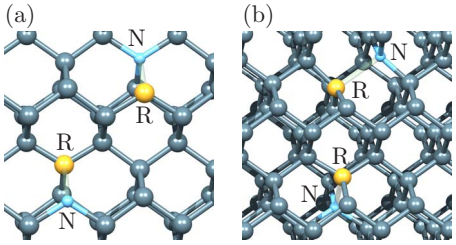

FIG. 11. (Color online) Schematics of the N9N and N10N complexes in diamond in the neutral charge state. Colors and orientation are as in Fig. 1.

above what we find to be the ground-state structure. On the basis of the current simulations it is therefore not possible to confirm or refute the proposition that NOC-1 has the specific form suggested in Ref. 19. All we may conclude is that it is plausible that such a structure might result in a paramagnetic defect.

IV. DISCUSSION

A. Total energies

The calculated total energies as a function of increasing separation rapidly converge to a value indistinguishable from that of two isolated P1 centers. Where there is a binding energy (i.e., the energy of the pair is lower than twice the energy of a P1 center), this reflects a chemical passivity or rebonding alluded to above. In particular, the total energies of N4N, N7aN, N7bN, N9N, and N10N all deviate from the sum of two P1 centers by less 0.1 eV. In line with the formation of additional bonding interactions, N1N, N2N, N3N, N5N, N6N, and N8N are bound by 3.6, 0.3, 0.3, 1.2, 0.1, and 1.4 eV, respectively.

For the positively charged cases, N1N, N2N, N5N, and N8N are bound by 1.7, 0.2, 0.3, and 0.2 eV, respectively, with all other structures having a binding energy less than 0.1 eV.

Finally, we note that for the 2+ charge state (for which we uniformly find the two N atoms to be on site), there is a simple Coulomb repulsion which diminishes with increasing distance. We find that no pairs are bound in the 2+ charge state.

B. Electrical activity: why are the dissociated pairs in the positive charge state?

The N1, W7, N4, M2, and M3 EPR centers assigned to separated nitrogen pairs are seen in an ionized state without the need for optical excitation. This may suggest a mechanism exists for the transfer of charge to some other site in the lattice. The types of diamond involved are generally plastically deformed and therefore it is plausible that in proximity to the nitrogen are carbon radical sites associated with point or line defects. We have previously shown[41] that native defects containing dangling bonds, such as vacancies and self-interstitials, give rise to rather deep acceptor levels, and in particular lower in the band gap than the donor levels of N_s^0. In addition, vacancy aggregates which have been linked to the brown coloration in these plastically deformed diamonds are linked with an acceptor level in the lower half of the band gap.[42]

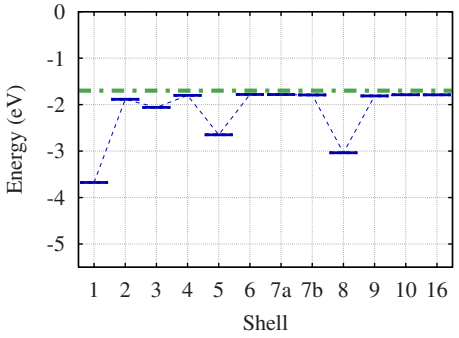

FIG. 12. (Color online) Plot of the variation in donor (dashed line) with shell number. The zero of energy is fixed at E_c, and the levels plotted as the ionization energy relative to this fixed point. The horizontal dot-dashed line at −1.7 eV shows the location of the donor level of isolated N_s^0.

Figure 12 shows the trend in the location of the donor level as a function of the shell number for the N pair using the marker method.[24] The dips in the donor levels correlate closely with the configurations which show the strongest chemical rebonding effects, as one might expect. Indeed, for those centers where all atoms are fully coordinated in the neutral charge state the donor levels lie relatively deep in the gap. This applies to N1N and N8N, and to a lesser extent N3N and N5N. For other separations the donor levels lie in the upper part of the band gap, close to that of the P1 center, and are therefore prone to ionization in the presence of carbon dangling bonds.

We note that the large structural changes in N8N systems mean that the second ionization level is predicted to lie *above* the first, rendering it thermodynamically unstable in the positive charge state. Thus even if this structure is present in the material, in equilibrium it would only exist in EPR-inactive forms, but optical excitation may lead to population of the metastable positive charge state.

C. Ferro- vs antiferromagnetic interactions for neutral pairs

For the neutral charge state, pairs of P1-centers might be thought to interact in one of two ways: $N_s^0(\uparrow)\ldots N_s^0(\downarrow)$ or $N_s^0(\uparrow)\ldots N_s^0(\uparrow)$. Indeed, since diamond often favors a high-spin state, the formation of paramagnetic pairs of P1-centers may be expected to be the norm.

However, the observations[19] seem to show the contrary, and the question remains as to why only three specific structures, NOC-1, NOC-2, and NOC-3, are seen in the $S=1$ spin state.

Our calculations give an explanation for the absence of paramagnetic N2N, N3N, N5N, N6N, N7bN, and N8N:

(i) For N3N, N5N and N8N there is a chemical rebonding which strongly stabilizes the $S=0$ configuration over the $S=1$.

(ii) For N2N and N6N, charge exchange between the two sites yield $N_s^+\ldots N_s^-$ complexes which naturally favor the $S=0$ configuration.

(iii) For N7bN an exchange splitting of around 0.1 eV in favor of the $S=0$ state is obtained, which may be traced to a very weak bonding interaction between the radical orbitals, but much weaker than N3N, N5N, and N8N as the sites are around 3 Å apart and not on neighboring C atoms.

This leaves N4N, N7aN, N9N, N10N, and more distant combination, matching the possible structures for the $S=1$ EPR centers as proposed in Ref. 19. Of these, N4N is the closest pairing which may yield a low-lying $S=1$ state. Although we find that the model for NOC-2 is around 60 meV above the lowest energy structure and spin state, this is within the margin for error, and the model remains plausible. Indeed, it is worth noting that the R2, $S=1$ EPR center corresponding to the [001]-split self-interstitial possesses a diamagnetic ground state around 50 meV below the paramagnetic state observed experimentally.[43] This ordering is also determined using computational methods similar to those employed in this study.[44] Therefore, even if the $S=1$ spin state is not the lowest energy configuration, it is not clear that this is inconsistent with experiment.

For the NOC-3 models, experiment is unable to distinguish between N7aN and N9N structures. The calculations suggest low-energy $S=1$ states for both configurations. For N7aN, the ground-state structure is not that proposed for NOC-3, whereas for N9N model structure for NOC-3 it is, although in both cases the margins of stability over other configurations are small. Therefore the simulations marginally favor a N9N structure for NOC-3, but the confidence level for such an assignment on the basis of these calculations must be low.

Indeed, the energies separating different orientations and spin states of N10N are also too small to draw any conclusions regarding NOC-1.

However, we note that it is perhaps surprising that both N7aN and N9N are not seen as separate centers, whereas N10N seems to be: all three cases are calculated to have more than one low energy $S=1$ configuration, and it is such a situation[19] that is the model for the average spectra labeled NOC-4.

Despite the lack of specificity in the assignment of the $S=1$ configurations, through a combination of charge-transfer and chemical rebonding, the calculations have accounted for the absence of many structures.

V. CONCLUSIONS

Given the importance of N as an impurity in diamond, the quantitative modeling of the hyperfine interactions in a range of N pair defects is a key result in the use of quantum-chemical simulations for the conclusive assignment of defect structures for experimentally obtained spectra. Our density functional simulations of nitrogen pairs in diamond have largely confirmed the atomistic models proposed from experiment with three qualifications. (i) for W24, we predict that the hyperfine interactions on the six equivalent carbon neighbors is opposite in sign from that on the N atoms. (ii) for N1, we propose a reassignment of the hyperfine interactions for nearby ^{13}C and the corresponding numbers of equivalent sites. (iii) for N4, in order to render the N atoms equivalent a rapid reorientation between two structures must be invoked, so that the low-temperature EPR spectra are the result of a thermal, or quantum-tunneling average of two systems where the N atoms are nonequivalent.

In addition, we predict values for the hyperfine interactions at the carbon sites where the majority of the spin density is located. Indeed, it is somewhat surprising that N1, W7, N4, M2, and M3 this radical site has not been seen, yet in the case of N1 many other carbon sites have.

We have also determined reasons for close by P1 centers not to combine in magnetically paired, $S=1$ combinations. Several form chemical bonds favoring an $S=0$ spin state, or undergo charge transfer forming $N_s^- \ldots N_s^+$ pairs. Of the remaining nearby pairs, generally an antiferromagnetic interaction, $N_s^0(\uparrow) \ldots N_s^0(\downarrow)$, is favored or there is a very small estimated exchange splitting.

Finally, we also note that N5N and N8N species introduce high-frequency local modes through the chemical reconstructions possible in the neutral charge state, and although the concentrations may be small, this provides a potential route to identification of N5N in the neutral analog of N4 and a second, highly stable form of N pairing in the N8N complex.

ACKNOWLEDGMENTS

We gratefully acknowledge discussions with J. M. Baker and V. Nadolinny in the preparation of this paper.

*j.p.goss@ncl.ac.uk

[1] R. Robertson, J. J. Fox, and A. E. Martin, Philos. Trans. R. Soc. London, Ser. A **232**, 463 (1934).
[2] J. P. Goss, B. J. Coomer, R. Jones, C. J. Fall, P. R. Briddon, and S. Öberg, Phys. Rev. B **67**, 165208 (2003).
[3] W. V. Smith, P. P. Sorokin, I. L. Gelles, and G. J. Lasher, Phys. Rev. **115**, 1546 (1959).
[4] A. T. Collins, M. Stanley, and G. S. Woods, J. Phys. D **20**, 969 (1987).
[5] S. C. Lawson, D. Fisher, D. C. Hunt, and M. E. Newton, J. Phys.: Condens. Matter **10**, 6171 (1998).
[6] G. Davies, Nature (London) **290**, 40 (1981).
[7] G. Davies, J. Phys. C **9**, L537 (1976).
[8] J. A. van Wyk and J. H. N. Loubser, J. Phys. C **16**, 1501 (1983).
[9] O. D. Tucker, M. E. Newton, and J. M. Baker, Phys. Rev. B **50**, 15586 (1994).
[10] M. Ya. Shcherbakova, E. V. Sobolev, N. D. Samsonenko, and V. K. Aksenov, Sov. Phys. Solid State **11**, 1104 (1969).
[11] A. Cox, M. E. Newton, and J. M. Baker, J. Phys.: Condens. Matter **4**, 8119 (1992).
[12] M. Ya. Shcherbakova, E. V. Sobolev, and V. A. Nadolinny, Sov. Phys. Dokl. **204**, 851 (1972).

[13] J. H. N. Loubser and A. C. J. Wright, J. Phys. D **6**, 1129 (1973).
[14] M. E. Newton and J. M. Baker, J. Phys.: Condens. Matter **3**, 3591 (1991).
[15] R. M. Mineeva, A. V. Speransky, S. V. Titkov, and N. G. Zudin, Phys. Chem. Miner. **34**, 53 (2007).
[16] R. M. Mineeva and A. V. Speransky, Appl. Magn. Reson. **28**, 355 (2005).
[17] M. Ya. Shcherbakova, E. V. Sobolev, V. A. Nadolinnyi, and V. K. Aksenov, Sov. Phys. Dokl. **20**, 725 (1975).
[18] C. M. Welbourn, Solid State Commun. **26**, 255 (1978).
[19] V. A. Nadolinny, A. P. Yelisseyev, J. M. Baker, D. J. Twitchen, M. E. Newton, A. Hofstaetter, and B. Feigelson, Phys. Rev. B **60**, 5392 (1999).
[20] J. P. Goss, R. J. Eyre, and P. R. Briddon, J. Phys.: Condens. Matter **20**, 085217 (2008).
[21] R. Jones and P. R. Briddon, in *Identification of Defects in Semiconductors*, Semiconductors and Semimetals, edited by M. Stavola (Academic Press, Boston, 1998), Vol. 51A, Chap. 6.
[22] M. J. Rayson and P. R. Briddon, Comput. Phys. Commun. **178**, 128 (2008).
[23] J. P. Perdew, K. Burke, and M. Ernzerhof, Phys. Rev. Lett. **77**, 3865 (1996).
[24] J. P. Goss, M. J. Shaw, and P. R. Briddon, in *Theory of Defects in Semiconductors*, Topics in Applied Physics, edited by David A. Drabold and Stefan K. Estreicher (Springer, Berlin/Heidelberg, 2007), Vol. 104, pp. 69–94.
[25] C. Hartwigsen, S. Goedecker, and J. Hutter, Phys. Rev. B **58**, 3641 (1998).
[26] D. A. Liberman, Phys. Rev. B **62**, 6851 (2000).
[27] H. J. Monkhorst and J. D. Pack, Phys. Rev. B **13**, 5188 (1976).
[28] M. J. Shaw, P. R. Briddon, J. P. Goss, M. J. Rayson, A. Kerridge, A. H. Harker, and A. M. Stoneham, Phys. Rev. Lett. **95**, 105502 (2005).
[29] P. E. Blöchl, Phys. Rev. B **50**, 17953 (1994).
[30] B. Hetényi, F. De Angelis, P. Giannozzi, and R. Car, J. Chem. Phys. **115**, 5791 (2001).
[31] We use values of I and μ_N of 1/2 and 0.70240 for ^{13}C, 1 and 0.430 60 for ^{14}N, and 1/2 and −0.283 10 for ^{15}N, taken from *CRC Handbook of Chemistry and Physics*, 77 ed., edited by D. R. Lide (CRC Press, Boca Raton, Florida, USA, 1996).
[32] R. Farrer, Solid State Commun. **7**, 685 (1969).
[33] G. Henkelman, B. P. Uberuaga, and H. Jónsson, J. Chem. Phys. **113**, 9901 (2000).
[34] G. Henkelman and H. Jónsson, J. Chem. Phys. **113**, 9978 (2000).
[35] Spherical-polar angles, (θ, ϕ) are given with θ the polar angle relative to [001], and the azimuth from [100], quoted in degrees.
[36] C. A. J. Ammerlaan, in *Semiconductors, Impurities and Defects in Group IV Elements and III–V Compounds*, Landolt-Börnstein New Series, edited by O. Madelung and M. Schultz (Springer, Berlin, 1990), Vol. III22B.
[37] We have perturbed the structure by displacing all atoms in random directions by up to 0.5 Å and rerelaxed to establish that symmetry constraints are not producing artificial energy minima. This small distortion does not exclude the possibility of more extensive rearrangements such as reconstructions or the production of carbon radicals, but does establish if the structure obtained is a local minimum in energy in the absence of any symmetry constraints. To test for other configurations, such as the location of carbon radications, relaxations are performed starting from structures where appropriate C-N bonds are either formed or broken.
[38] M. E. Newton and J. M. Baker, J. Phys.: Condens. Matter **3**, 3605 (1991).
[39] S. Dannefaer, A. Pu, and D. Kerr, Diamond Relat. Mater. **10**, 2113 (2001); S. Dannefaer and K. Iakoubovskii, J. Phys.: Condens. Matter **20**, 235225 (2008).
[40] J. H. N. Loubser and J. A. van Wyk, MRS Symposia Proceedings No. 43 (Materials Research Society, Warrendale, 1985), p. 587.
[41] J. P. Goss, P. R. Briddon, S. J. Sque, and R. Jones, Diamond Relat. Mater. **13**, 684 (2004).
[42] L. S. Hounsome, R. Jones, P. M. Martineau, D. Fisher, M. J. Shaw, P. R. Briddon, and S. Öberg, Phys. Rev. B **73**, 125203 (2006).
[43] D. C. Hunt, D. J. Twitchen, M. E. Newton, J. M. Baker, T. R. Anthony, W. F. Banholzer, and S. S. Vagarali, Phys. Rev. B **61**, 3863 (2000).
[44] J. P. Goss, B. J. Coomer, R. Jones, T. D. Shaw, P. R. Briddon, M. Rayson, and S. Öberg, Phys. Rev. B **63**, 195208 (2001).